# Supporting Information

# Long-Circulating Amphiphilic Doxorubicin for Tumor Mitochondria-Specific Targeting

Jingchao Xi[†], Meng Li[†], Benxin Jing[†], Myunggi An[†], Chunsong Yu[†], Cameron B. Pinnock[‡], Yingxi Zhu[†], Mai T. Lam[‡], Haipeng Liu*[,†,§,∥]

[†]Department of Chemical Engineering and Materials Science, Wayne State University, Detroit, Michigan 48202, United States

[‡]Department of Biomedical Engineering, Wayne State University, Detroit, Michigan 48202, United States

[§]Department of Oncology, Wayne State University, Detroit, Michigan 48201, United States

[∥]Tumor Biology and Microenvironment Program, Barbara Ann Karmanos Cancer Institute, Detroit, Michigan 48201, United States

*Corresponding author E-mail: haipeng.liu@wayne.edu

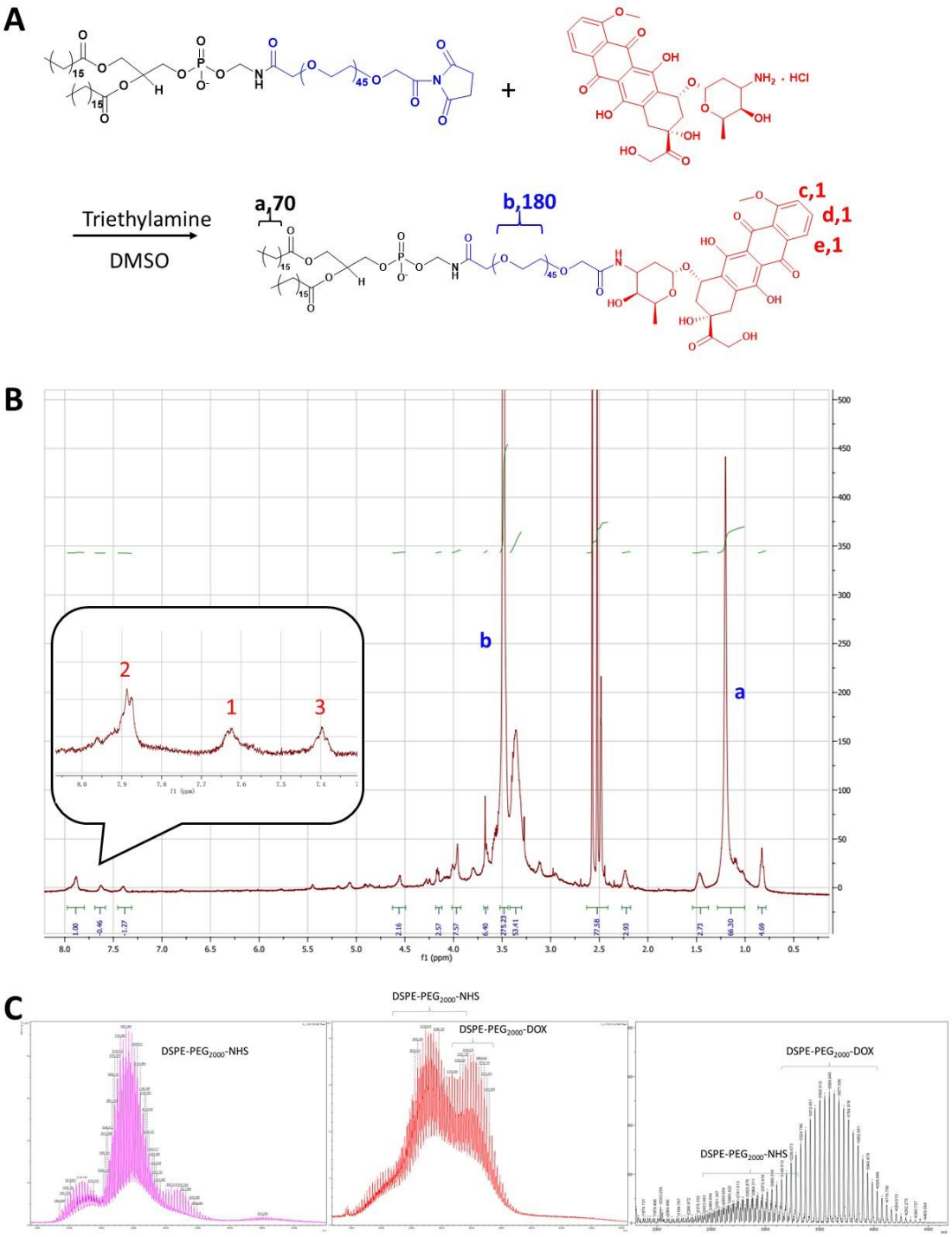


**Figure S1. Synthesis (A), NMR (B) and Mass-Spec (C) characterization of amph-DOX.** (A) Amph-DOX was synthesized by conjugating of doxorubicin hydrochloride (DOX) to DSPE-PEG$_{2000}$-NHS. (B) $^{1}$H-NMR spectra of amph-DOX. The proton peaks of DOX (c, d, and e) and DSPE-PEG (a, b) were observed at 8.5~7.0 ppm and 0.9~3.6 ppm, respectively. (C) MALDI-TOF spectrometry analysis of DSPE-PEG$_{2000}$-NHS (left), crude reaction mixture (middle) and DSPE-PEG$_{2000}$-DOX after HPLC purification (right).

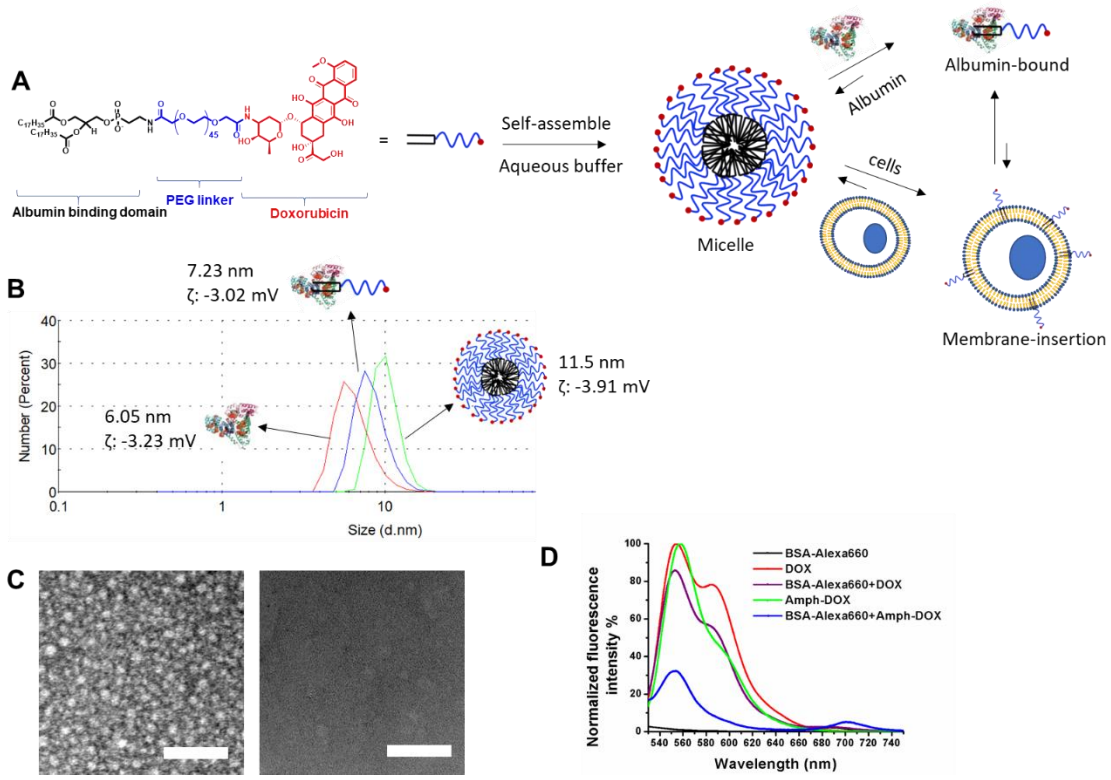


**Figure S2. Self-assemble, membrane-insertion, and albumin-binding properties of amph-DOX.** (A) In aqueous solution, spherical micelles are self-assembled from amph-DOX with a DOX-PEG corona and a lipid core. In the presence of albumin and cells, the micelle structure is disrupted by binding to albumin (albumin hitchhiking), or inserting on plasma membrane (membrane insertion). The structure of lipid-polymer (e.g., the length of lipid and PEG) and albumin concentration govern the equilibrium partitioning between albumin binding state or membrane insertion state. Current structure ($DSPE\text{-}PEG_{2000}$) was optimized for albumin-binding based on our previous finding.[1] At high concentrations of albumin (e.g., 640 μM in blood), the equilibrium strongly favors albumin-binding. (B) Hydrodynamic size distributions and zeta potential obtained by dynamic size scattering, for samples of pure amph-DOX micelle, albumin, and albumin-bound amph-DOX. (C) Transmission electron microscopy (TEM) image of amph-DOX micelles (left) and albumin-bound amph-DOX (right). Scale bar: 100 nm. (D) Albumin-binding properties of Doxorubicin hydrochloride (DOX) and amph-DOX assayed by fluorescence resonance energy transfer (FRET).

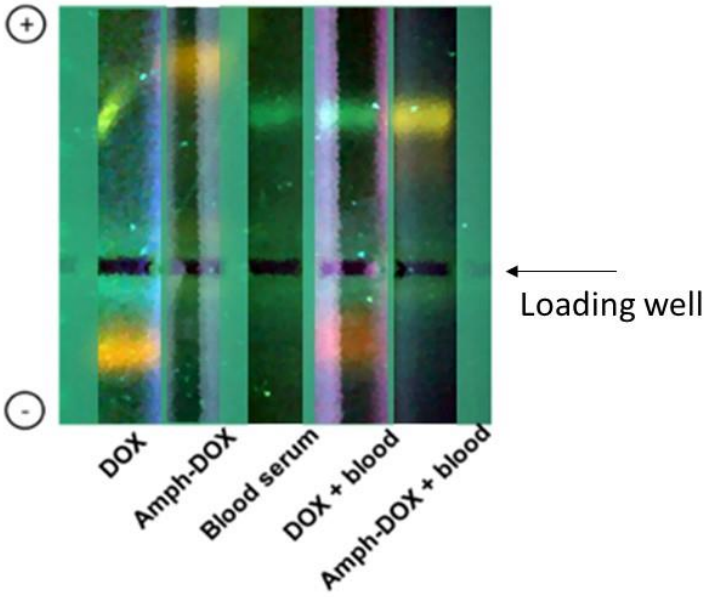


**Figure S3. Amph-DOX binds to albumin in blood.** Mouse blood samples were incubated with 0.5 μM DOX or amph-DOX for 4 h, after separating blood cells by centrifugation, sera were analyzed by gel electrophoresis. The color and contrast of each lane was adjusted by Photoshop.

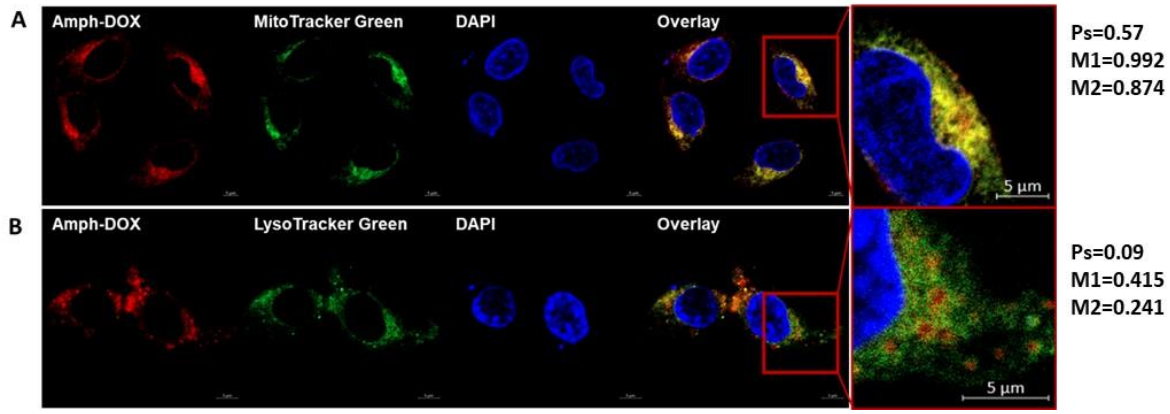


**Figure S4. Confocal microscope characterization of B16F10 cells showing intracellular distribution of amph-DOX (concentration of 1 μM) at 4 h.** B16F10 cells were treated with amph-DOX (red) and stained for mitochondria (green) by MitoTracker Green (**A**) or LysoTracker Green (**B**). Cell nuclei were stained with DAPI (blue). Scale bar = 5 μm.

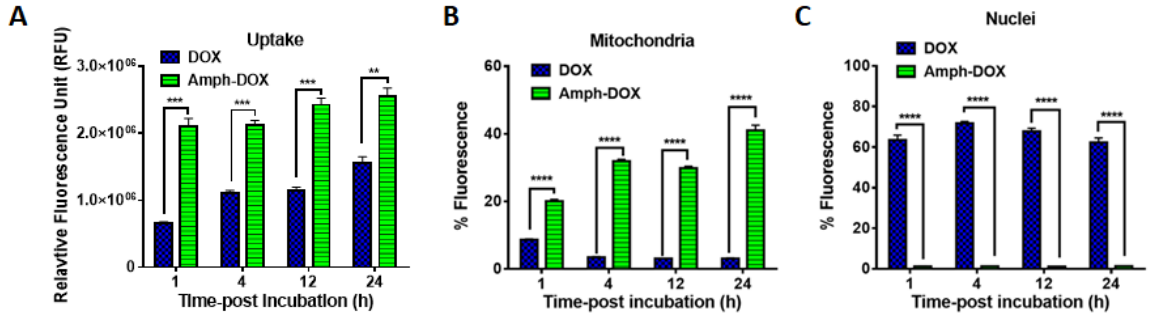


**Figure S5. Quantification of DOX or amph-DOX in (*A*) overall uptake, (*B*) mitochondria and (*C*) nuclei of B16F10 cells.** 1 x $10^8$ cells were incubated with 10 μM DOX or amph-DOX for 1, 4, 12, 24 h. Mitochondria and nuclei were isolated by isolating kits and the uptake were quantified by fluorescence spectroscopy after solvent extraction. The DOX concentrations were normalized to the percentage in total amount within the cells. Data show the mean values ± SEM. *, P <0.05; **, P <0.01; ***<0.001; ****<0.0001 by unpaired Student's t test.

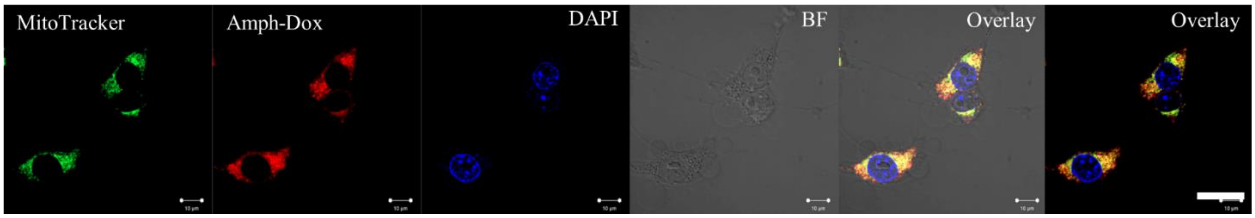


**Figure S6. Mitochondria accumulation of amph-DOX in 4T1 cells.** 4T1 cells were treated with amph-Dox (red) and stained for mitochondria (green) by MitoTracker Green. Cell nuclei were stained by DAPI (blue).

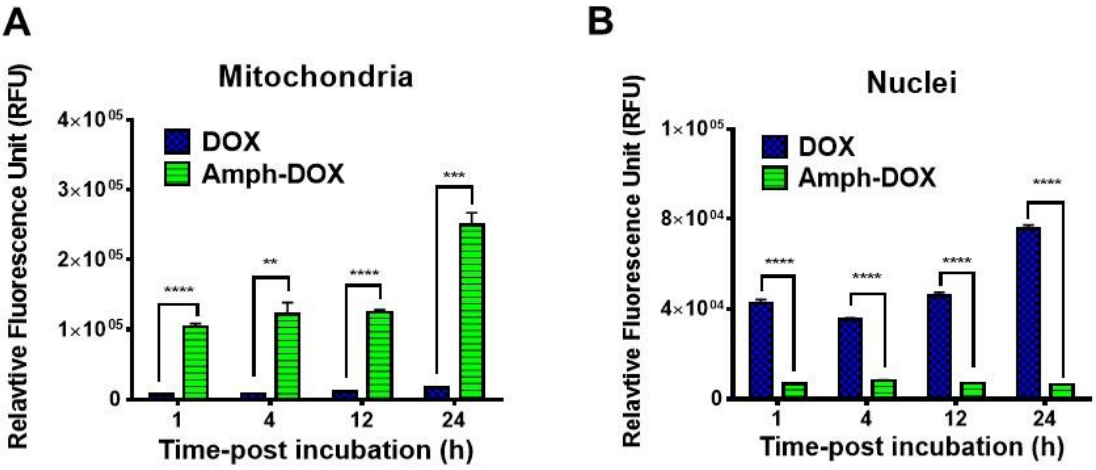


**Figure S7**. **Quantification of DOX or amph-DOX in (A) mitochondria and (B) nuclei of NCI/ADR-RES cells.** 1 x $10^8$ cells were incubated with 10 μM DOX or amph-DOX for 1, 4, 12, 24 h. Mitochondria and nuclei were isolated by isolating kits and quantified by fluorescent measurements. Data show the mean values ± SEM. *, P <0.05; **, P <0.01; ***<0.001; ****<0.0001 by unpaired Student's t test.

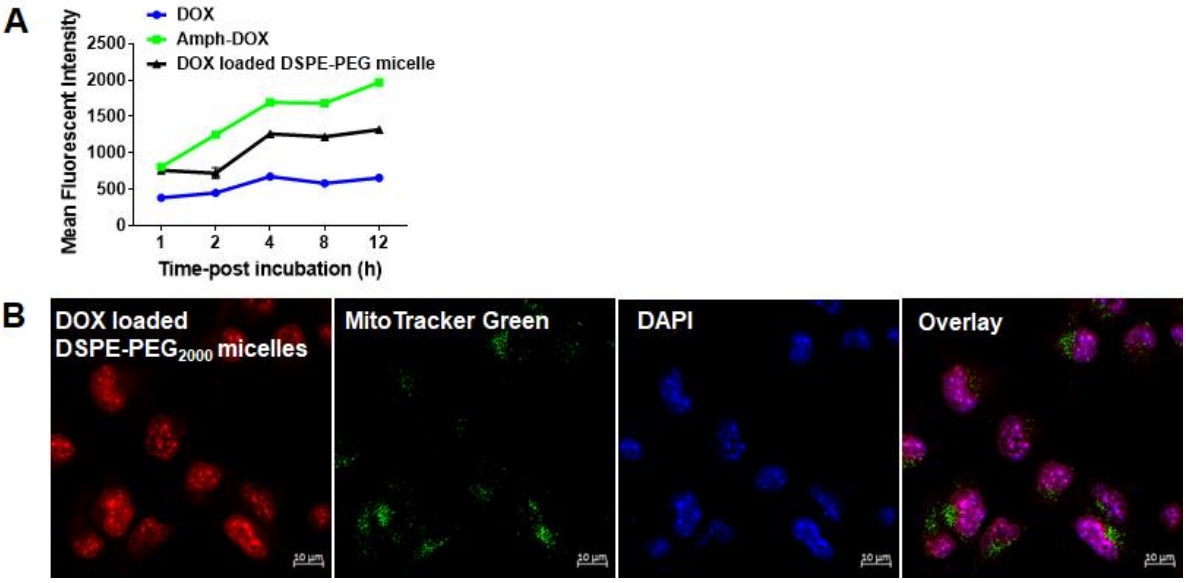


**Figure S8. Cellular uptake (A) and intracellular distribution (B) of doxorubicin encapsulated DSPE-PEG$_{2000}$ micelles.**

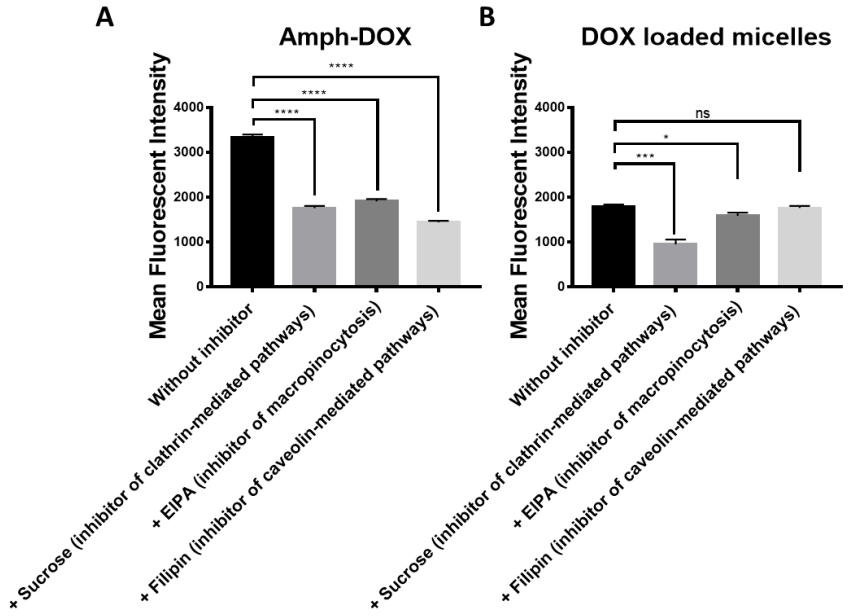


**Figure S9. Cellular uptake mechanisms of amph-DOX and micelle DOX in 10% FBS.** B16F10 cells were incubated with amph-DOX or micelle DOX in the presence of different inhibitors, cellular uptake was measured by flow cytometry. Culturing cells with filipin, the caveolae transport inhibitor, or sucrose, the clathrin-mediated inhibitor, or EIPA (inhibitor of macropinocytosis) resulted in 50-65% reduction of amph-DOX uptake (A), suggesting multiple mechanisms are involved in the uptake of amph-DOX. In contrast, the uptake of DOX loaded DSPE-PEG2000 micelles was primarily affected by clathrin-inhibitor (B).

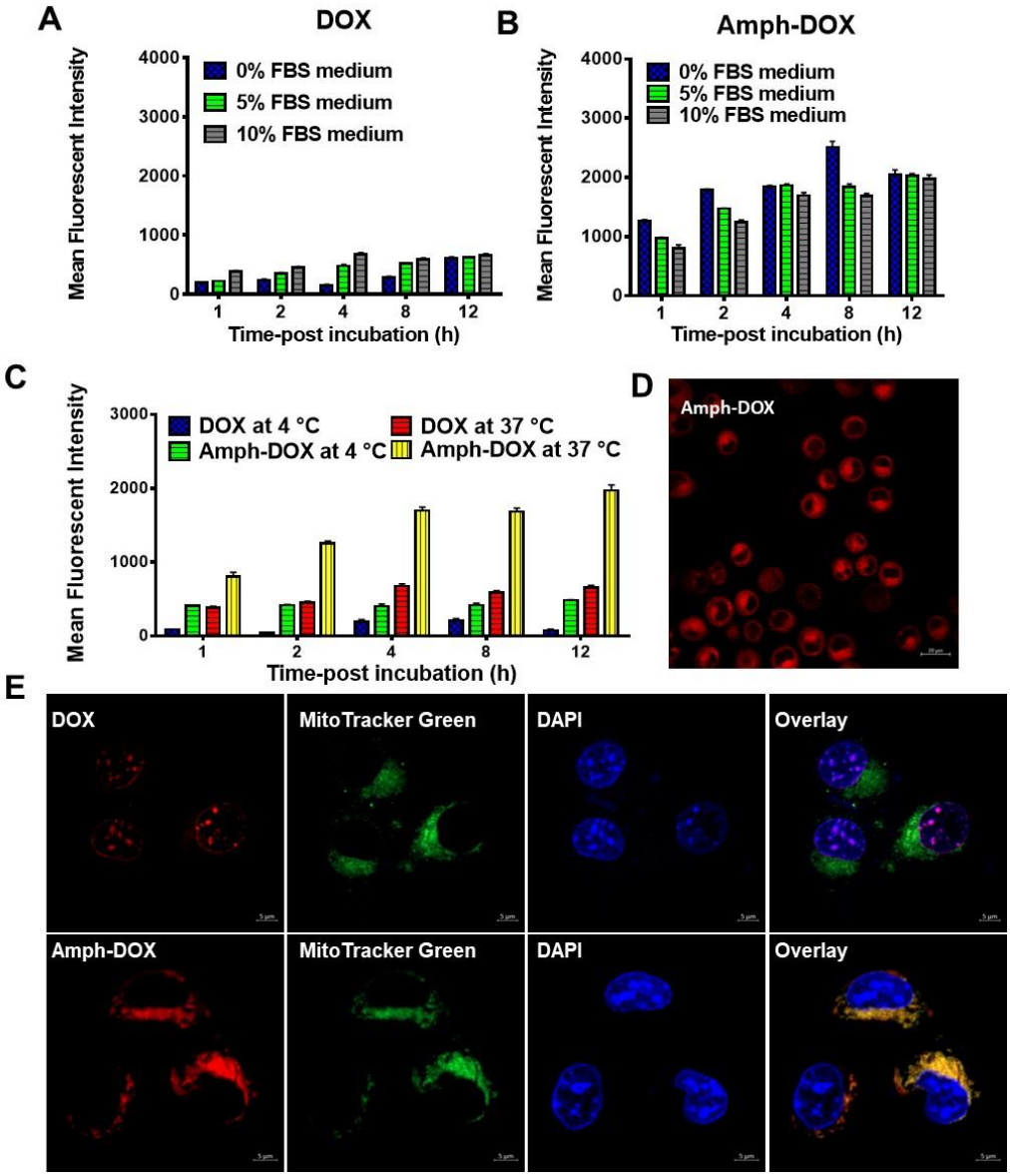


**Figure S10. Effect of serum on amph-DOX uptake and subcellular location.** B16F10 cells uptake of free DOX (A) and amph-DOX (B) in different concentrations of FBS was examined by flow cytometry. (C), DOX or amph-DOX were incubated with B16F10 cells in 10% FBS at 4 °C or 37 °C. Uptake was quantified by flow cytometry. (D), B16F10 cells were incubated with amph-DOX in FBS free medium at 4 °C, cells were analyzed by confocal microscope. (E), intracellular distribution of DOX and amph-DOX in B16F10 cells in the absence of FBS. Cells were treated with free DOX, and amph-DOX (red) for 4 hours and stained for mitochondria (green) by MitoTracker Green. Cell nuclei were stained with DAPI (blue). Scale bar = 5 μm.

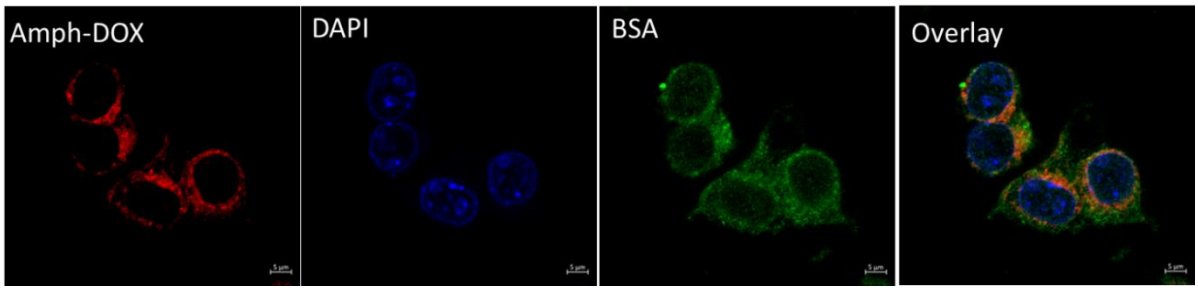


**Figure S11. Confocal microscope characterization of B16F10 cells showing intracellular distribution of amph-DOX and BSA-Alexa fluor647 at 4 h.** B16F10 cells were treated with amph-DOX (red) precomplexed with BSA-Alexa fluor647 (green) for 4 hours. Cell nuclei were stained with DAPI (blue). Scale bar = 5 µm.

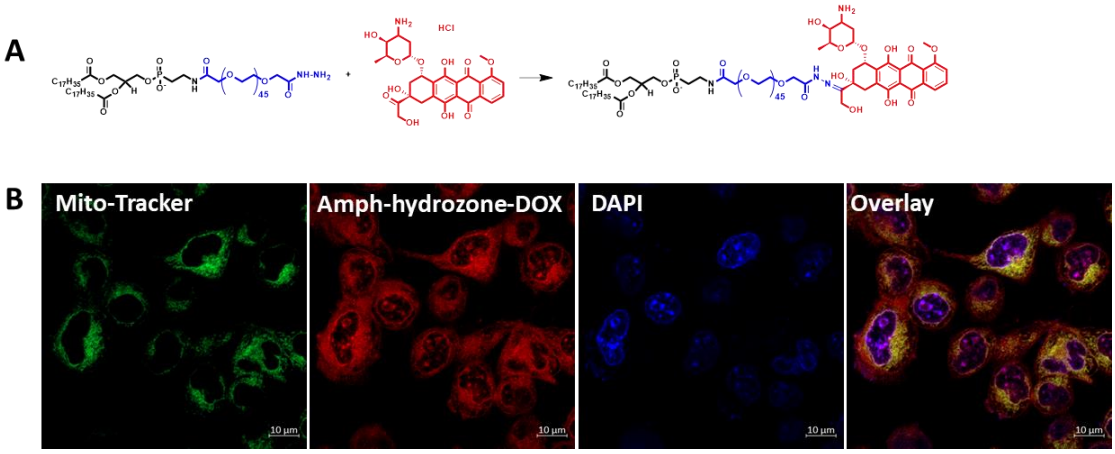


**Figure S12. Synthesis (A) and intracellular distribution (B) of amph-DOX with a pH sensitive hydrozone linkage.** (A), DOX was conjugated to DSPE-$PEG_{2000}$ via a pH-sensitive hydrazone bond to release DOX in an acidic environment inside cancer cells. (B), DOX fluorescence in nuclei as well as in mitochondria was observed. The mitochondria accumulation of this pH-sensitive amph-hydrozone-DOX is perhaps due to the incomplete cleavage of hydrozone bond under endosomal pH.[2] Another possibility is that cargos transported via caveolae-dependent route (**Fig. S9**) are delivered to caveosomes instead of lysosomes. Along this route, the pH is maintained neutral and no degradative end-station is reached (Curr Pharm Biotechnol 2001; 2:1-17). Nevertheless, the partial nuclear accumulation of amph-hydrozone-DOX strongly suggest that DOX is not released in our original amph-DOX (non-cleavable) design.

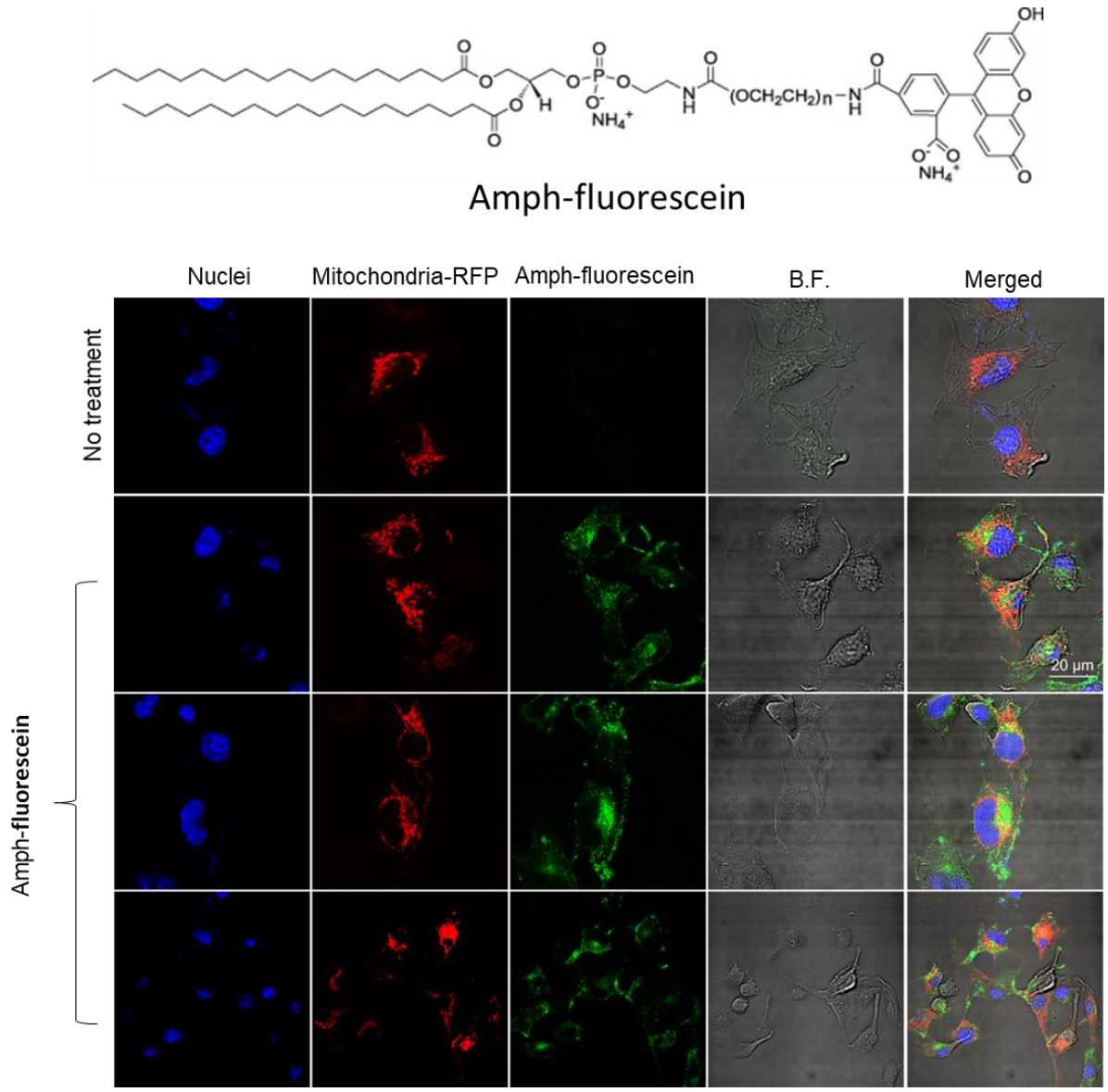


**Figure S13. Structure of amph-Fluorescein and its intracellular distribution.** B16F10 cells were incubated with amph-Fluorescein for 24 h and imaged to detect its intracellular distribution. No mitochondria accumulation was observed.

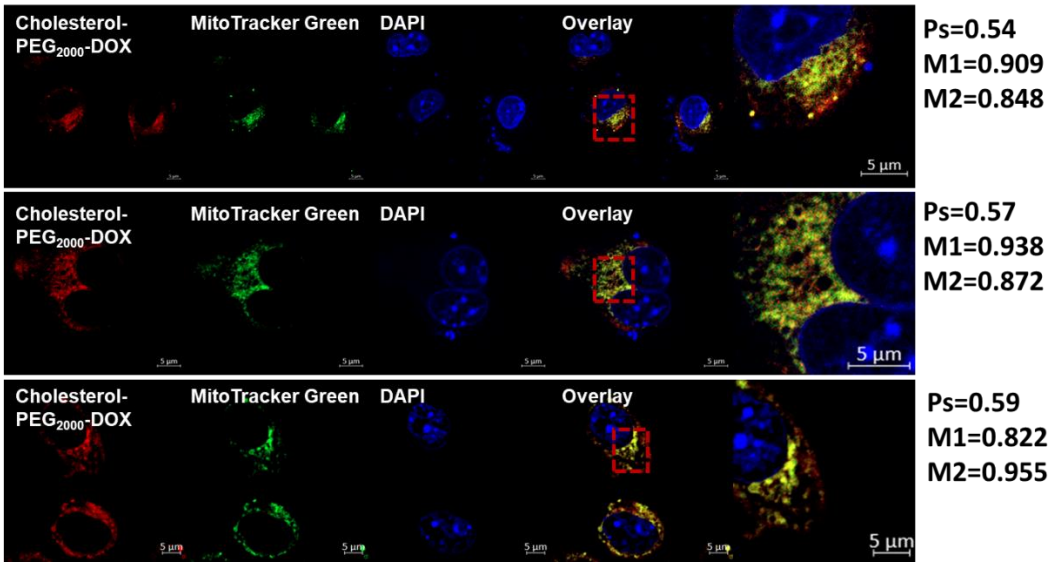


**Figure S14. Subcellular location of Cholesterol-PEG$_{2000}$-DOX in B16F10 cells.** Cells were seeded to 6-well plate (1× $10^5$ cells per well) and incubated at 37 ℃ for overnight. The cell medium incubated with DOX and amph-DOX at a final concentration of 1.0 μM for 4 hours. Cells were treated with Cholesterol-PEG$_{2000}$-DOX (red) and stained for mitochondria (green) by Mito-Tracker Green. Cell nuclei were stained with DAPI (blue). Scale bar = 5 μm.

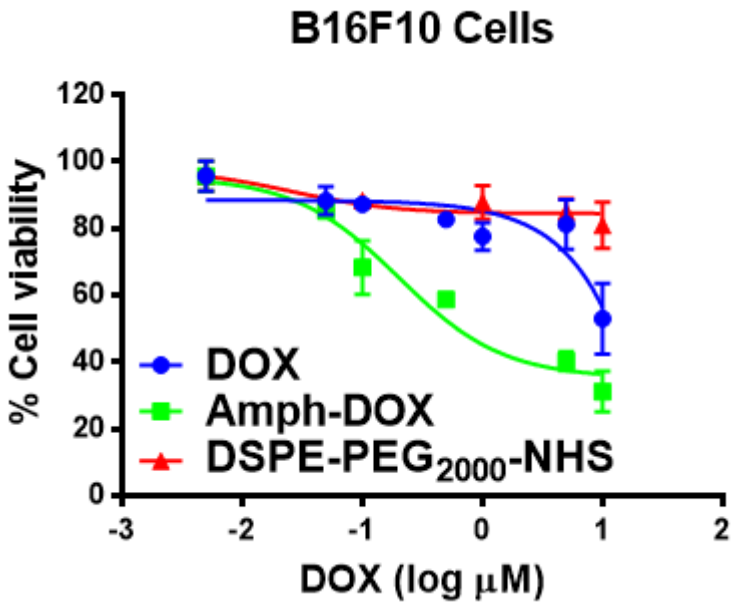


**Figure S15. *In vitro* antitumor activity of DOX, amph-DOX and DSPE-PEG$_{2000}$-NHS.** B16F10 cancer cells were incubated with DOX, DSPE-PEG$_{2000}$-NHS or amph-DOX with varies concentration for 24h.

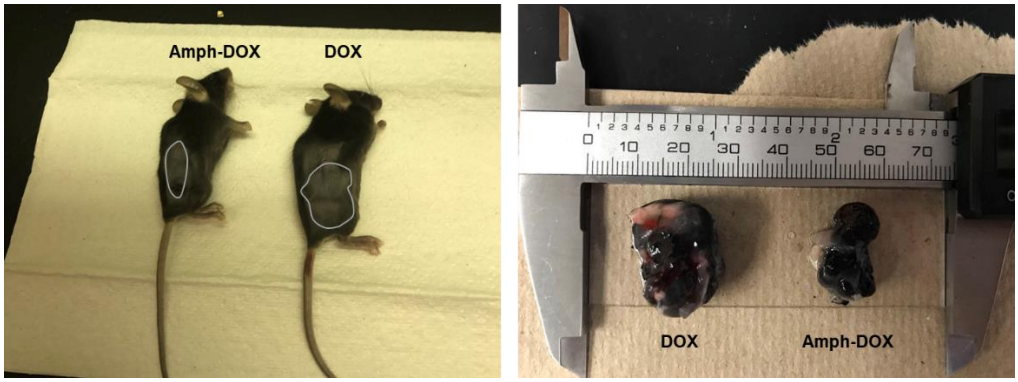


**Figure S16. Tumor photographs of whole animals (day 15 after tumor inoculation) and after isolation.**

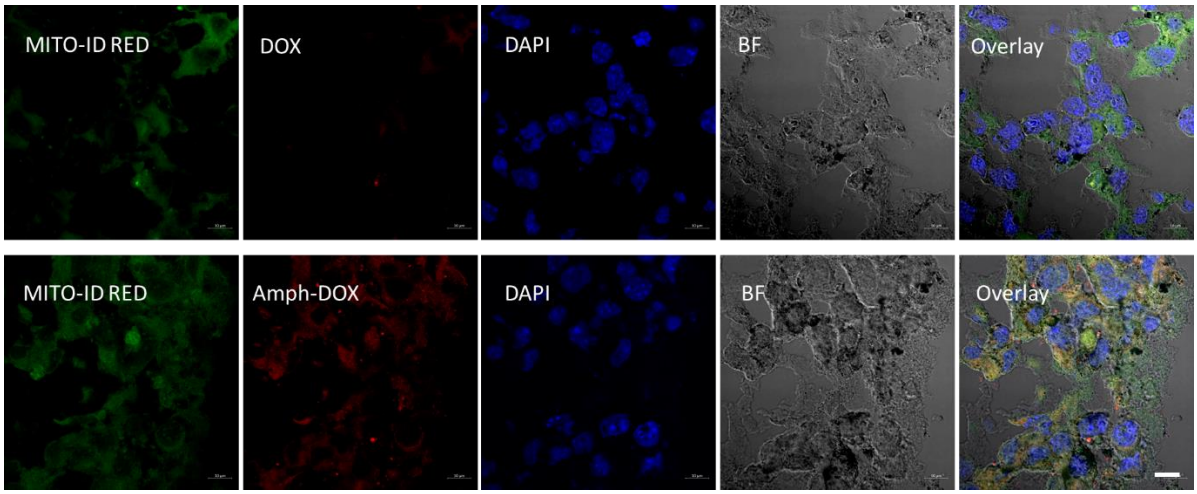


**Figure S17. Confocal laser scanning microscopy (CLSM) images of frozen sections of B16F10 tumor tissues showing prolonged and enhanced tumor accumulation of amph-DOX at 48 h post injection.** Tumor tissues were isolated 48 h after DOX or amph-DOX injection. Tumor sections were labeled and imaged. Images show DOX (red,), mitochondria (green, stained with MITO-ID RED), nuclei (blue, stained by DAPI) and overlay (scale bar = 5 µm).

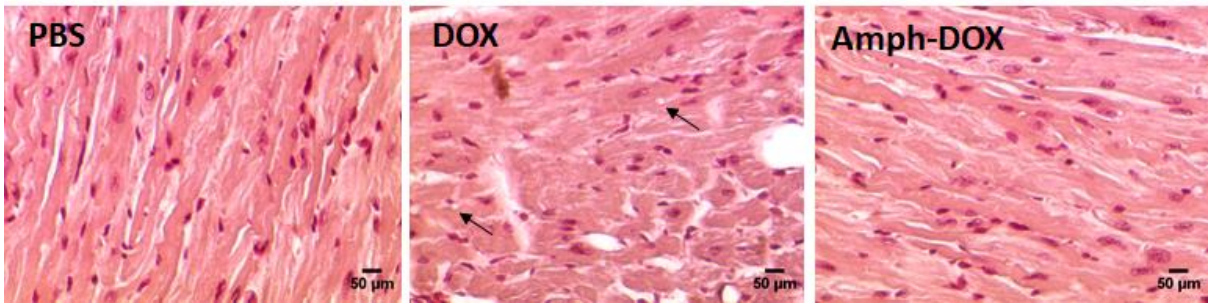


**Figure S18. Representative photomicrographs of heart sections of DOX and amph-DOX treated mice stained with H&E.** H&E staining of cardiac muscle sections from tumor-free mice receiving the same treatment scheme as outlined in Fig. 6C. Vacuole structures are indicated with black arrows.

**Table S1. Pearson's Correlation Coefficients and Manders coefficients**

| | DOX | | | Amph-DOX | |
|---|---|---|---|---|---|
| | Ps | M1/M2 | | Ps | M1/M2 |
| Mitochondria | -0.26 | 0.196/0.039 | | 0.52 | 0.901/0.750 |
| | -0.19 | 0.083/0.020 | | 0.52 | 0.773/0.975 |
| | -0.04 | 0.133/0.083 | | 0.57 | 0.874/0.992 |
| Nuclei | 0.63 | 0.709/0.937 | | -0.06 | 0.463/0.014 |
| | 0.62 | 0.675/0.873 | | -0.01 | 0.517/0.004 |
| | 0.56 | 0.811/0.946 | | -0.06 | 0.897/0.331 |

**Table S2. HPLC gradient for purification of amph-Dox.**

| Time(min) | Methanol (%) | 0.1 M TEAA (%) |
|---|---|---|
| 0.00 | 50.0 | 50.0 |
| 10.00 | 100.0 | 0.0 |
| 15.00 | 100.0 | 0.0 |
| 15.01 | 0.0 | 100.0 |
| 20.00 | 0.0 | 100.0 |

## References

1. Liu, H.; Moynihan, K. D.; Zheng, Y.; Szeto, G. L.; Li, A. V.; Huang, B.; Van Egeren, D. S.; Park, C.; Irvine, D. J. Structure-Based Programming of Lymph-Node Targeting in Molecular Vaccines. *Nature* **2014,** *507*, 519-522.

2. Kalia, J.; Raines, R. T. Hydrolytic Stability of Hydrazones and Oximes. *Angewandte Chemie (International ed. in English)* **2008,** *47*, 7523-7526.